Microelectronic Engineering 86 (2009) 1230–1233

Contents lists available at ScienceDirect

Microelectronic Engineering

journal homepage: www.elsevier.com/locate/mee

A mass-balanced through-wafer electrostatic *x*/*y*-scanner for probe data storage

J.B.C. Engelen [a,*], H.E. Rothuizen [b], U. Drechsler [b], R. Stutz [b], M. Despont [b], L. Abelmann [a], M.A. Lantz [b]

[a] MESA+ and Impact Research Institutes, University of Twente, Hogekamp 6206, P.O. Box 217, 7500 AE Enschede, The Netherlands
[b] IBM Research, Zürich Research Laboratory, 8803 Rüschlikon, Switzerland

ARTICLE INFO

Article history:
Received 30 September 2008
Received in revised form 10 November 2008
Accepted 21 November 2008
Available online 3 December 2008

Keywords:
Probe storage
MEMS
DRIE
Electrostatic actuator
Comb drive
Finite-element analysis (FEA)

ABSTRACT

In this work we describe the design, fabrication, and testing of a mass-balanced planar *x*/*y*-scanner designed for parallel-probe data storage applications. The scanner is actuated by comb drives, whose finger shape is improved using finite-element analysis to increase the force output. A mass-balancing concept is used for in-plane shock resistance; in the out-of-plane direction passive shock resistance is achieved using 1:40 aspect-ratio springs that are fabricated by deep reactive ion etching through the full thickness of a 400 μm wafer. A prototype device is presented and its performance is reported.

1. Introduction

Parallel-probe data storage is a promising candidate for future storage applications. By using atomic-force-microscope-like probes, a high data density can be reached (>1 Tb/in^2), while a high data rate is achieved by operating many probes in parallel [1,2]. By manufacturing these systems with batch micro-fabrication technology, the devices can be made small and low cost. This makes probe-based storage attractive for mobile storage applications. However, mobile applications introduce additional challenges. First, the storage system should be robust against vibration and shock, and second, it must operate on a restricted power budget.

Several scanners for probe storage systems, using varying physical actuation principles, can be found in the literature, including comb drives [3,4]; however, these lack a vibration and shock resistance mechanism and the structures are too thin to maintain a stable nano-scale gap between probe-tip and recording media. A design reported by Lantz et al. [5] with electromagnetic voice coil actuation uses a mechanical scheme to increase vibration resistance, greatly alleviating the demands on the actuator force and controller bandwidth. The feedback system uses thermal sensors to obtain nanometer resolution. In this work, we start from this design and explore the use of comb drives instead of coils and magnets. Previously, increased comb drive force by tapering fingers has been reported by Rosa et al. [6]. Here we investigate a tapered finger shape using two-dimensional electrostatic finite-element (FE) simulations.

The total power consumption of the electromagnetic scanner of [5] is dominated by track follow rather than seek operations because seek operations are much shorter. When reading the outermost track (50 μm displacement), the electromagnetic scanner's *x*-axis consumes 20 mW on average and the *y*-axis 60 mW continuously, which is almost a third of the SD flash memory card power budget of 300 mW. The power consumption can be reduced by optimizing the scanner stiffness and the actuator design, however, power is always required to maintain a non-equilibrium position. An advantage of comb drives compared to electromagnetic actuation is that, neglecting leakage, no energy is consumed to maintain the actuator position. The comb drive's force is caused by charge instead of current flow; once a comb drive is put at a certain position by charging the combs, no more energy has to be supplied to maintain its position. Thus during reading, since one axis is standing still and the other is moving slowly, energy consumption is potentially much lower compared to electromagnetic actuation. A disadvantage is the high voltage required to operate comb drives, typically many times the standard voltage available in a mobile storage device. DC/DC conversion is used commonly in mobile devices (12 V for Flash memory and 28 V for LCD display); and conversion from 3 V to 380 V has been demonstrated for MEMS applications [7]. In our design, we have assumed that 150 V is a reasonable upper limit.

2. Design, modeling and optimization

Our scanner design, shown in Fig. 1, features a scan table to carry the storage medium, and two comb drive actuators that

* Corresponding author.
E-mail address: j.b.c.engelen@utwente.nl (J.B.C. Engelen).

0167-9317/$ - see front matter © 2008 Elsevier B.V. All rights reserved.
doi:10.1016/j.mee.2008.11.032

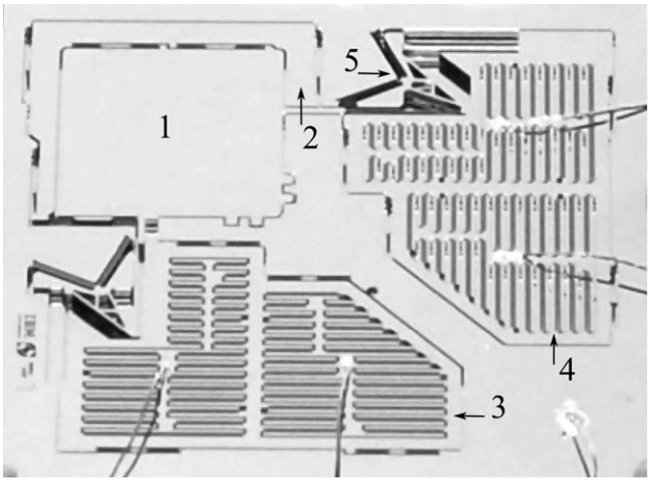

Fig. 1. Photograph of the assembled scanner (2 × 2 cm). 1: scan table, 2: C-bracket, 3: *x* comb drives, 4: *y* comb drives, 5: pivoting element.

generate force in the *x* and *y* directions. A comb drive actuator consists of a translator that can move and is electrically grounded, and two fixed stators to which a voltage can be applied to induce a force in either the positive or negative direction. To achieve vibration and shock resistance, a mass-balancing concept is adopted from [5]. The design offers shock resistance in the planar *x* and *y* directions while being compliant for actuation. The scan table and actuator translators are mechanically linked via pivoting elements, such that scan table and translator are restricted to move in opposite directions. When the pivot ratio matches the inverse ratio of the scan table and translator masses, the equally directed inertial forces of a linear shock are canceled, providing enhanced linear shock resistance [5].

The scan table is supported by a C-bracket suspended to the fixed outer frame, to decouple movement in the *x* and *y* directions. In the *y* direction, the scan table and the C-bracket move as one; in the *x* direction, only the scan table moves. This means that the moving mass in the *x* direction is lower than in the *y* direction. Because the comb drive translator masses are equal to the scan table plus C-bracket mass, a 1:1 pivot ratio is used in the *y* direction. In the *x* direction, a 1:1.36 pivot ratio is used (i.e. the scan table moves a factor 1.36 more than the corresponding translator).

A large out-of-plane stiffness for passive vibration rejection is achieved by etching the device, including the spring suspension, through the full thickness of the wafer (400 μm). For a uniform etch load, the whole mask design is defined with a fixed etch trench width of 20 μm and a minimum structure width of 15 μm. The resulting trench width after etching is 25 μm and the minimum structure width is 10 μm. Wide openings are made by drawing a 20 μm wide trench along a contour, with a drop-out piece in the center. With these rules, the minimum finger width is 10 μm and the gap between comb drive fingers after etching is 25 μm. The openings within the comb drives have no dropout pieces.

An important figure of merit for investigating vibration and shock resistance is the maximum available force at every displacement point,

$$F_{\text{avail}}(x) = F_{\text{comb}}(x) - kx, \tag{1}$$

where F_{comb} is the force generated by the comb drive at a certain voltage, *k* the spring constant of the suspension, and *x* the displacement. Although mass-balancing is used, there must always be an available force 'reserve' to compensate for vibration and shock forces due to mass mismatches and rotational shocks.

The generated force equals $F_{\text{comb}}(x) = \frac{1}{2}V^2\frac{\partial C}{\partial x}$, where *V* is the applied voltage, *C* the capacitance, and *x* the comb drive displacement. We have investigated two finger shape designs using finite-element (FE) simulations (Fig. 2). The first design uses straight fingers while the second design has a tapered finger shape to increase the generated force [6]. For straight fingers, the necessary change in capacitance $\frac{\partial C}{\partial x}$ is caused by increasing finger overlap; for tapered fingers, an extra term due to the decreasing gap distance between fingers adds to the capacitance change, hence an increase in force. To prevent snap-in, there is a minimum required separation between the tips of the fingers and the comb base. Then with the required 50 μm maximum displacement, a finger length of 110 μm and 25 μm overlap between fingers at zero displacement were chosen.

The result of the FEM analysis is shown in Fig. 3. It is important to note that for negative displacements, although F_{comb} decreases (the overlap between fingers is 25 μm, so the fingers are com-

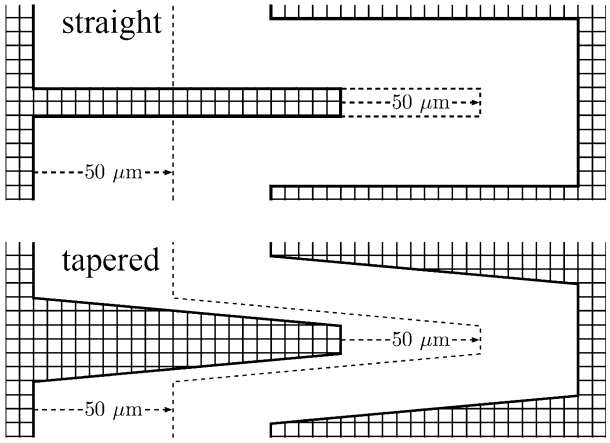

Fig. 2. The two investigated finger geometries. The dashed outline shows the geometry at 50 μm displacement.

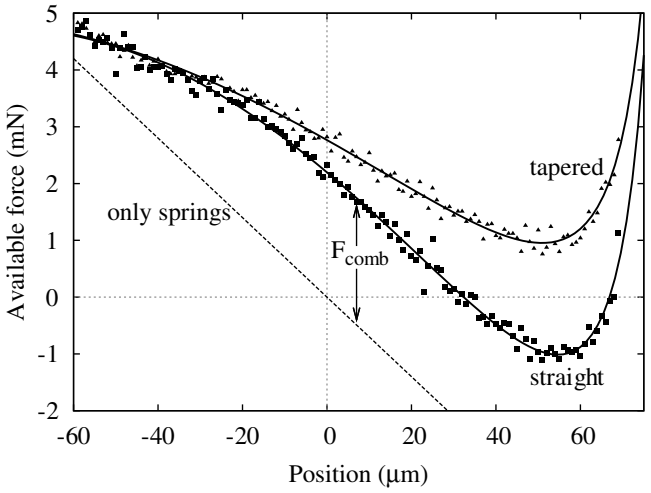

Fig. 3. The maximum available force (=$F_{\text{comb}} - kx$) in the positive direction as calculated by 2 D electrostatic FE simulations for straight and tapered finger shapes (V = 150 V; k = 70 N/m; 698 finger pairs). The solid lines are 'guides to the eye'. The dashed curve shows the force from the suspension springs only.

pletely disengaged for $x < -25$ μm), the springs add to the available force in this region. The minimum of the curve lies not in the region where the fingers are disengaged, but in fact in the region where the comb drive is close to snap-in. The straight finger design reaches a maximum displacement of about 30 μm, with zero available force; the tapered fingers would be able to reach a displacement of about 50 μm before snapping in, with 1 mN available force. The prototype presented in this work uses the tapered finger shape and utilizes 731/698 comb finger pairs for the +/− directions respectively.

3. Fabrication and assembly

The scanner is fabricated from a 400-μm single-crystal, highly doped silicon wafer using a deep-trench-etching process, etching through the wafer in 165 min with an aluminum etch stop. A side view of the comb fingers is given in Fig. 4a, showing the etch profile.

The comb drive stators are completely surrounded by the translators; therefore, to prevent the stators from falling out at the end of the etch process, several break-out pieces (see Fig. 4b) connect the stators mechanically to the translators. After etching, individual scanner chips are separated from the wafer and glued to insulating base plates. The break-out pieces are then removed to provide electrical isolation between stators and translators. After gluing to the baseplate, electric contact is made to the device by connecting copper wires using conducting epoxy.

4. Experimental results and discussion

The driven frequency response and the displacement versus voltage curves of the fabricated prototype are shown in Fig. 5. To ensure that the driving force is a sine wave without harmonics, we used a waveform with the form $\sqrt{\sin(t)+1}$. The data were measured using a UMECH motion analyzer [8].

The measured resonance frequencies for the x and y axes are 147 and 133 Hz, respectively, in good agreement with the values of 148 and 130 Hz predicted by mechanical FE simulations. The effective spring constants extracted from these simulations were 100 and 70 Nm^{-1} for the x and y axes respectively. A stable translator displacement of 38 μm at 156 V was measured for the x axis, whereas the y axis moved 38 μm at 119 V, see Figs. 5c and 5d. Although the displacement versus applied voltage curve corresponds well with the FE simulation (shown as dotted curves in Figs. 5c and 5d), snap-in occurred earlier than expected.

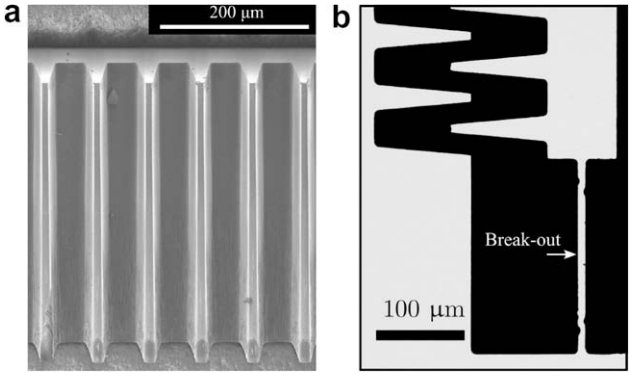

Fig. 4. (a) SEM image of comb drive side view showing the increase in finger width toward the back of the wafer; (b) microscope image of the front side, showing the break-out piece between stator and translator. The break-out piece is designed with small indents on both ends for easier breaking.

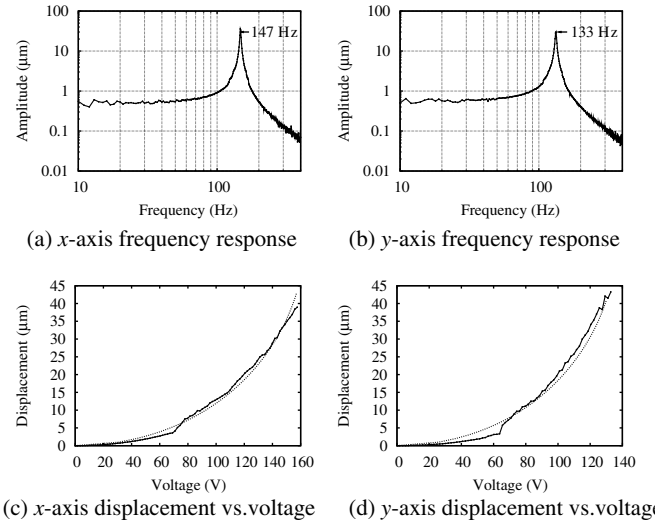

(a) x-axis frequency response (b) y-axis frequency response

(c) x-axis displacement vs.voltage (d) y-axis displacement vs.voltage

Fig. 5. Actuator frequency response to $\sqrt{\sin(2\pi ft)+1}$ drive voltage; and displacement versus voltage (the dotted curves are FE simulation results). The features in the displacement curves between 60 and 70 V are measurement errors caused by video processing.

The maximum generated force calculated from the measured maximum displacement was 3.8 mN (at 156 V) and 2.7 mN (at 119 V) for the x and y axes, respectively.

For both axes, snap-in occurred earlier than expected, limiting the translator displacement to 38 μm. A possible explanation is the slightly angled etch profile, resulting in a thicker finger outline on the backside of the wafer and a reduced gap distance between finger tip and comb base. The maximum scan table displacement in the x and y directions is 52 μm and 38 μm, respectively. The difference between the two axes results from the different pivot ratios used.

The footprint of the total device is 3 mm larger in both directions than the 16×17 mm^2 total area of the electromagnetic scanner reported in [5], reducing the areal efficiency from 17% to 12 %. The electrostatic scanner is however potentially thinner depending on the chosen base plate thickness and the particular electromagnetic scanner design. An advantage of the electrostatic scanner is that, if it is fabricated from a SOI wafer, gluing and break-out pieces are no longer necessary, enabling simpler mass fabrication compared to the electromagnetic scanner where the coils and magnets are glued manually.

5. Conclusion

The presented scanner prototype shows that the use of comb drives in a shock resistant nanopositioner is promising for mobile storage applications. Scan table displacements of 52 μm at 156 V for the x axis and 38 μm at 119 V for the y axis were measured. Tapered fingers greatly improve performance compared to standard straight fingers, resulting in about 70% larger maximum displacement in the presented case.

Acknowledgement

This research was supported by the Technology Foundation STW, applied science division of NWO and the technology program of the Ministry of Economic Affairs under project number TES.06369. We would like to thank Henk van Wolferen for the SEM images.

References

[1] R.J. Cannara, B. Gotsmann, A. Knoll, U. Dürig, Nanotechnology 19 (2008) 395305.
[2] A. Pantazi et al., IBM J. Res. Dev. 52 (2008) 493–511.
[3] Y. Lu, C.K. Pang, J. Chen, H. Zhu, J.P. Yang, J.Q. Mou, G.X. Guo, B.M. Chen, T.H. Lee, in: Proceedings International Conference on Advanced Intelligent Mechatronics, 2005, pp. 19–24.
[4] C.-H. Kim, H.-M. Jeong, J.-U. Jeon, Y.-K. Kim, J. MEMS 12 (2003) 470–478.
[5] M.A. Lantz, H.E. Rothuizen, U. Drechsler, W. Haberle, M. Despont, J. MEMS 16 (2007) 130–139.
[6] M.A. Rosa, S. Dimitrijev, H.B. Harrison, Electron. Lett. 34 (1998) 1787–1788.
[7] J.-F. Saheb, J.-F. Richard, M. Sawan, R. Meingan, Y. Savaria, Analog Integr. Circ. Signal Process. 53 (2007) 27–34.
[8] UMECH MEMS Motion Analyzer, Umech Technologies. Watertown, MA.